

# Semiclassical study of electronically nonadiabatic dynamics in the condensed-phase: Spin-boson problem with Debye spectral density

Haobin Wang, Xueyu Song,<sup>a)</sup> David Chandler, and William H. Miller  
*Department of Chemistry, University of California, and Chemical Sciences Division,  
Lawrence Berkeley National Laboratory, Berkeley, California 94720*

(Received 20 August 1998; accepted 4 December 1998)

The linearized semiclassical initial value representation (LSC-IVR) [H. Wang, X. Sun and W. H. Miller, *J. Chem. Phys.* **108**, 9726 (1998)] is used to study the nonadiabatic dynamics of the spin-boson problem, a system of two electronic states linearly coupled to an infinite bath of harmonic oscillators. The spectral density of the bath is chosen to be of the Debye form, which is often used to model the solution environment of a charge transfer reaction. The simulation provides a rather complete understanding of the electronically nonadiabatic dynamics in a broad parameter space, including coherent to incoherent transitions along all three axes (the  $T$ -axis, the  $\eta$ -axis, and the  $\omega_c$ -axis) in the complete phase diagram and the determination of rate constants in several physically interesting regimes. Approximate analytic theories are used to compare with the simulation results, and good agreement is found in the appropriate physical limits. © 1999 American Institute of Physics. [S0021-9606(99)51010-6]

## I. INTRODUCTION

Although considerable progress has been made over the last few years in the rigorous quantum mechanical calculation of thermal (also microcanonical) rate constants for chemical reactions,<sup>1</sup> these methods are at present applicable without approximation to molecular systems involving only a few (3–4) atoms. The primary reason is that the finite basis used in such calculations grows exponentially as the number of degrees of freedom increases. Some kind of approximation is thus necessary in order to deal with complex molecular systems, those with many degrees of freedom. An attractive approach, the semiclassical initial value representation<sup>2</sup> (SC-IVR), is now undergoing a rebirth of interest<sup>3–10</sup> in this regard. The SC-IVR replaces the quantum mechanical trace in the formally exact rate expressions by a phase space average over the initial conditions of classical trajectories, for which Monte Carlo techniques can be used. The integrand of the phase space average is oscillatory, however, and it is an active research problem to develop more efficient algorithms to deal with this aspect of an SC-IVR calculation.

In lieu of a full SC-IVR treatment, a linearized approximation to it (the LSC-IVR) was suggested in a recent paper<sup>11</sup> and found to give excellent results for a model condensed phase problem, a one-dimensional double well potential linearly coupled to an infinite bath of harmonic oscillators. The approximation, which linearizes the phase difference in the integrand, leads to an extremely simple computational procedure, one that is only slightly more expensive than a routine classical molecular dynamics simulation. It has also been shown<sup>12</sup> that the LSC-IVR can be applied to electronically nonadiabatic processes by using the Meyer–Miller model<sup>13,14</sup> to provide a dynamically consistent treatment of

electronic and nuclear degrees of freedom. For the three model nonadiabatic scattering problems used by Tully<sup>15</sup> to test surface-hopping models, it was found that LSC-IVR performed quite well, even correctly describing Stuckelberg oscillations (interferences between nonadiabatic transitions). The LSC-IVR was also applied to the spin-boson problem,<sup>12</sup> i.e., a two level system linearly coupled to an infinite bath of harmonic oscillators,<sup>16–18</sup> and it reproduced quite accurately quantum path integral results<sup>19,20</sup> for the case of an Ohmic (with an exponential cutoff) bath spectral density.

These encouraging results demonstrate the usefulness and feasibility of the LSC-IVR for treating complex molecular systems. Previous work<sup>21</sup> has established the fact that the LSC-IVR describes the short time (of order  $\beta\hbar$ ) behavior of quantum time correlation functions correctly—thus accurately describing quantum effects (tunneling, etc.) in a transition state theory approximation<sup>22</sup> for reaction rate constants—but the longer time dynamics is essentially that given by classical mechanics. The success in previous applications of the LSC-IVR suggests that quantum coherence effects, which are often quite important for a small molecule gas phase reaction, are quenched by the condensed phase environment. Moreover, it will be shown in this paper that if the nonadiabatic states are treated via the dynamically consistent method suggested by McCurdy, Meyer and Miller,<sup>13,14</sup> the exact quantum coherence effects for the two level system are fully reproduced by the LSC-IVR approximation. Bearing in mind its simplicity and ease of practical implementation, the LSC-IVR is expected to be applicable to a wide class of complex chemical reactions.

In this paper, we apply the LSC-IVR approximation to the popular spin-boson problem, a system of two electronic states linearly coupled to an infinite bath of harmonic oscillators, but with a significantly different bath spectral density

<sup>a)</sup>Current address: Department of Chemistry, Iowa State University, Ames, IA 50011.

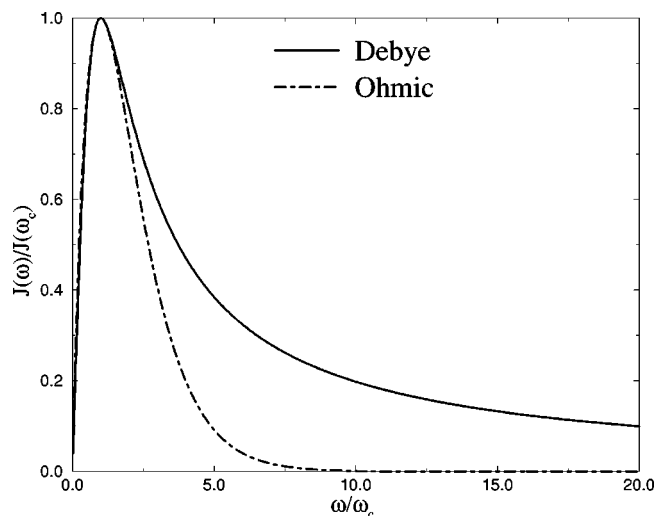


FIG. 1. Debye (solid line) and Ohmic (dashed line) spectral densities.

than considered before.<sup>12</sup> Specifically, the two-state (diabatic) representation of the Hamiltonian is

$$\hat{H} = \begin{bmatrix} H_B - H_c & \Delta \\ \Delta & H_B + H_c \end{bmatrix}, \quad (1.1a)$$

where the bath Hamiltonian  $H_B$  and the system-bath coupling  $H_c$  are written conveniently in terms of the mass-weighted coordinates and momenta as

$$H_B = \sum_j \frac{1}{2} (P_j^2 + \omega_j^2 Q_j^2), \quad (1.1b)$$

$$H_c = \sum_j c_j Q_j. \quad (1.1c)$$

The central property of the bath is its spectral density<sup>17</sup>

$$J(\omega) = \frac{\pi}{2} \sum_j \frac{c_j^2}{\omega_j} \delta(\omega - \omega_j), \quad (1.2)$$

which characterizes the effect of the bath on transitions between the electronic states (e.g., electron transfer in the condensed phase). In this work, the spectral density is chosen in the so-called Debye form

$$J_D(\omega) = \frac{\eta \omega_c \omega}{\omega^2 + \omega_c^2}. \quad (1.3)$$

[Equation (1.3) is actually of Ohmic form with a Lorentzian cutoff; the name convention ‘‘Debye’’ is adopted here because the condensed phase media characterized by this spectral density exhibits Debye dielectric relaxation.<sup>23</sup>] The two parameters which characterize the spectral density, the characteristic bath frequency  $\omega_c$  and the coupling strength  $\eta$ , are related to other physical quantities:  $1/\omega_c = \tau_L$  is the longitudinal relaxation time, and  $2\eta$  is the reorganization energy in charge transfer theory. As shown in Fig. 1, the Debye spectral density spans a much broader frequency range than the usual Ohmic case (with an exponential cutoff)

$$J_O(\omega) = \eta \omega e^{-\omega/\omega_c}, \quad (1.4)$$

and thus presents a greater challenge for numerical simulations.

Spectral densities of real chemical/biological systems are of course much more complicated, but they should nevertheless have some general features in common: at small frequencies, they scale linearly versus  $\omega$  [i.e., the Ohmic form  $J(\omega) \sim \eta \omega$ ], whereas for large frequencies they should decay in the form of a power law [i.e.,  $J(\omega) \sim \eta (\omega_c/\omega)^n$ ,  $n > 0$ ]. Despite its simple form, the Debye spectral density captures these essential features. Theoretical/computational approaches capable of treating it are thus expected to be applicable to more complex realistic spectral densities. It is our hope, therefore, that the work presented in this paper will permit critical examinations of several approximate analytic theories for charge transfer processes and also foster future analytical development.

Section II first summarizes the LSC-IVR procedure for the calculation of the time correlation functions, and Sec. III gives specifics of the present calculation for the spin-boson problem. Section IV discusses the results and their comparisons with approximate analytic theories, and Sec. V concludes.

## II. SUMMARY OF THEORY

In the semiclassical initial value representation<sup>2-10</sup> (SC-IVR), the time evolution operator for a  $f$ -dimensional system is approximated by

$$e^{-i\hat{H}t/\hbar} = \int d\mathbf{p}_0 \int d\mathbf{q}_0 \left[ \det \left( \frac{\partial \mathbf{q}_t}{\partial \mathbf{p}_0} \right) / (2i\pi\hbar)^f \right]^{1/2} \times e^{iS_t(\mathbf{p}_0, \mathbf{q}_0)/\hbar} |\mathbf{q}_t\rangle \langle \mathbf{q}_0|, \quad (2.1)$$

where  $\mathbf{q}_t(\mathbf{p}_0, \mathbf{q}_0)$  is the trajectory determined by initial conditions  $(\mathbf{p}_0, \mathbf{q}_0)$  and  $S_t(\mathbf{p}_0, \mathbf{q}_0)$  the classical action integral along it. [The phase factor  $e^{-i\pi\nu_t/2}$ , where  $\nu_t$  is the Maslov index, is included in Eq. (2.1) as part of the pre-exponential square root.] Thus, for the general time correlation function of the form

$$C_{AB}(t) = \text{tr}[\hat{A} e^{i\hat{H}t/\hbar} \hat{B} e^{-i\hat{H}t/\hbar}] \\ = \int d\mathbf{q} \int d\mathbf{q}' \int d\mathbf{q}_0 \int d\mathbf{q}_0' \langle \mathbf{q}_0' | \hat{A} | \mathbf{q}_0 \rangle \\ \times \langle \mathbf{q}_0' | e^{i\hat{H}t/\hbar} | \mathbf{q}' \rangle \langle \mathbf{q}' | \hat{B} | \mathbf{q} \rangle \langle \mathbf{q} | e^{-i\hat{H}t/\hbar} | \mathbf{q}_0 \rangle, \quad (2.2)$$

the SC-IVR result gives the following general result:

$$C_{AB}(t) = (2\pi\hbar)^{-f} \int d\mathbf{q}_0 \int d\mathbf{q}_0' \int d\mathbf{p}_0 \int d\mathbf{p}_0' \langle \mathbf{q}_0' | \hat{A} | \mathbf{q}_0 \rangle \\ \times \langle \mathbf{q}_t' | \hat{B} | \mathbf{q}_t \rangle \exp\{i[S_t(\mathbf{p}_0, \mathbf{q}_0) - S_t(\mathbf{p}_0', \mathbf{q}_0')]/\hbar\} \\ \times \left[ \det \left( \frac{\partial \mathbf{q}_t}{\partial \mathbf{p}_0} \right) \right]^{1/2} \left[ \det \left( \frac{\partial \mathbf{q}_t'}{\partial \mathbf{p}_0'} \right) \right]^{1/2}, \quad (2.3)$$

where  $\mathbf{q}_t = \mathbf{q}_t(\mathbf{p}_0, \mathbf{q}_0)$  and  $\mathbf{q}_t' = \mathbf{q}_t(\mathbf{p}_0', \mathbf{q}_0')$ .

The linearized SC-IVR (LSC-IVR) approximation is obtained by making a sum and difference change of integration variables,

$$\bar{\mathbf{p}}_0 = \frac{1}{2}(\mathbf{p}_0 + \mathbf{p}_0'), \quad \Delta\mathbf{p}_0 = \mathbf{p}_0 - \mathbf{p}_0', \quad (2.4a)$$

$$\bar{\mathbf{q}}_0 = \frac{1}{2}(\mathbf{q}_0 + \mathbf{q}_0'), \quad \Delta\mathbf{q}_0 = \mathbf{q}_0 - \mathbf{q}_0', \quad (2.4b)$$

and then expanding all relevant quantities to the first order in the difference variables  $\Delta\mathbf{p}_0$  and  $\Delta\mathbf{q}_0$ :

$$\mathbf{q}_t(\mathbf{p}_0, \mathbf{q}_0) \approx \bar{\mathbf{q}}_t + \frac{\partial \bar{\mathbf{q}}_t}{\partial \bar{\mathbf{p}}_0} \cdot \frac{\Delta\mathbf{p}_0}{2} + \frac{\partial \bar{\mathbf{q}}_t}{\partial \bar{\mathbf{q}}_0} \cdot \frac{\Delta\mathbf{q}_0}{2}, \quad (2.5a)$$

$$\mathbf{q}_t'(\mathbf{p}_0', \mathbf{q}_0') \approx \bar{\mathbf{q}}_t - \frac{\partial \bar{\mathbf{q}}_t}{\partial \bar{\mathbf{p}}_0} \cdot \frac{\Delta\mathbf{p}_0}{2} - \frac{\partial \bar{\mathbf{q}}_t}{\partial \bar{\mathbf{q}}_0} \cdot \frac{\Delta\mathbf{q}_0}{2}, \quad (2.5b)$$

$$\frac{\partial \mathbf{q}_t(\mathbf{p}_0, \mathbf{q}_0)}{\partial \mathbf{p}_0} \approx \frac{\partial \mathbf{q}_t'(\mathbf{p}_0', \mathbf{q}_0')}{\partial \mathbf{p}_0'} \approx \frac{\partial \bar{\mathbf{q}}_t}{\partial \bar{\mathbf{p}}_0}, \quad (2.5c)$$

$$\frac{\partial \mathbf{q}_t(\mathbf{p}_0, \mathbf{q}_0)}{\partial \mathbf{q}_0} \approx \frac{\partial \mathbf{q}_t'(\mathbf{p}_0', \mathbf{q}_0')}{\partial \mathbf{q}_0'} \approx \frac{\partial \bar{\mathbf{q}}_t}{\partial \bar{\mathbf{q}}_0}, \quad (2.5d)$$

$$\begin{aligned} S_t(\mathbf{p}_0, \mathbf{q}_0) - S_t(\mathbf{p}_0', \mathbf{q}_0') &\approx \frac{\partial S_t(\bar{\mathbf{p}}_0, \bar{\mathbf{q}}_0)}{\partial \bar{\mathbf{p}}_0} \cdot \Delta\mathbf{p}_0 + \frac{\partial S_t(\bar{\mathbf{p}}_0, \bar{\mathbf{q}}_0)}{\partial \bar{\mathbf{q}}_0} \cdot \Delta\mathbf{q}_0 \\ &= \bar{\mathbf{p}}_t \cdot \frac{\partial \bar{\mathbf{q}}_t}{\partial \bar{\mathbf{p}}_0} \cdot \Delta\mathbf{p}_0 + \bar{\mathbf{p}}_t \cdot \frac{\partial \bar{\mathbf{q}}_t}{\partial \bar{\mathbf{q}}_0} \cdot \Delta\mathbf{q}_0 - \bar{\mathbf{p}}_0 \\ &\quad \cdot \Delta\mathbf{q}_0, \end{aligned} \quad (2.5e)$$

where  $\bar{\mathbf{q}}_t = \mathbf{q}_t(\bar{\mathbf{p}}_0, \bar{\mathbf{q}}_0)$  and  $\bar{\mathbf{p}}_t = \mathbf{p}_t(\bar{\mathbf{p}}_0, \bar{\mathbf{q}}_0)$ . Our abbreviated notation is, for example, that  $\partial \bar{\mathbf{q}}_t / \partial \bar{\mathbf{p}}_0$  is the matrix  $(\partial \bar{\mathbf{q}}_t / \partial \bar{\mathbf{p}}_0)_{i,i'} = \partial \bar{q}_{t,i} / \partial \bar{p}_{t,i'}$ . The integration over the difference variables  $\Delta\mathbf{p}_0$  and  $\Delta\mathbf{q}_0$  can now be carried out<sup>11</sup> in Eq. (2.3) to give the final result of the LSC-IVR,

$$C_{AB}(t) = (2\pi\hbar)^{-f} \int d\mathbf{q}_0 \int d\mathbf{p}_0 A^w(\mathbf{q}_0, \mathbf{p}_0) B^w(\mathbf{q}_t, \mathbf{p}_t)^*, \quad (2.6)$$

where we have also dropped the ‘‘bars’’ over  $\mathbf{p}_0$  and  $\mathbf{q}_0$  since they no longer serve any purpose.  $A^w(B^w)$  is the Wigner/Weyl transform<sup>24</sup> of the operator  $\hat{A}(\hat{B})$ , which is defined as

$$A^w(\mathbf{q}, \mathbf{p}) = \int d\Delta\mathbf{q} e^{-i\mathbf{p} \cdot \Delta\mathbf{q}/\hbar} \left\langle \mathbf{q} + \frac{\Delta\mathbf{q}}{2} \left| \hat{A} \right| \mathbf{q} - \frac{\Delta\mathbf{q}}{2} \right\rangle. \quad (2.7)$$

If operators  $\hat{A}$  and  $\hat{B}$  are Hermitian (i.e., they correspond to some physical observable), their Wigner transforms are real,

$$A^w(\mathbf{q}, \mathbf{p})^* = A^w(\mathbf{q}, \mathbf{p}), \quad B^w(\mathbf{q}, \mathbf{p})^* = B^w(\mathbf{q}, \mathbf{p}), \quad (2.8)$$

and since this is true for all operators of interest to us we drop the complex-conjugate sign in Eq. (2.6).

It is clear that the linearized semiclassical initial value representation (LSC-IVR), Eq. (2.6), is much simpler than the full-blown SC-IVR. The real time propagation is purely classical, with the oscillatory part of the integrand merged into the Wigner distribution functions (the weighting functions)  $A^w(\mathbf{q}_0, \mathbf{p}_0)$  and  $B^w(\mathbf{q}_t, \mathbf{p}_t)$ . The procedure is only slightly more difficult than a standard classical trajectory calculation. Its limitation, as has been discussed elsewhere,<sup>21</sup> is that quantum effects in the dynamics are accurately described only for short time, with the longer time dynamics given by classical rather than quantum mechanics. For com-

plex molecular systems, such quantum interference effects in the long time dynamics are often quenched and the LSC-IVR therefore expected to provide an adequate description.

It should also be noted that Eq. (2.6), which we refer to as the LSC-IVR, is the classical limit of the Wigner equivalent expression of the trace, a result obtained previously by a variety of approaches.<sup>22,25–28</sup> The reason that we emphasize that this result arises from linearizing the SC-IVR expression, Eq. (2.3), is that this suggests how one can in principle improve the LSC-IVR, i.e., by going beyond this linearized approximation.

So far we have assumed that the Hamiltonian of the problem has a classical analog, as is the case for reactions occurring on a single electronic potential surface. The spin-boson problem studied in this paper, however, is a *nonadiabatic* process involving two electronic states/potential energy surfaces. The LSC-IVR formalism, Eq. (2.6), is thus not directly applicable to the Hamiltonian (1.1) due to its discretized form. Common approximations for treating nonadiabatic dynamics are the time-dependent self-consistent field (TDSCF) model<sup>29</sup> and the surface hopping model.<sup>30</sup> A more dynamically consistent treatment of electronic and nuclear degrees of freedoms can be obtained, however, by following the work of McCurdy, Meyer, and Miller,<sup>13,14</sup> and introducing classical degrees of freedom that model the finite number of discrete electronic states, the so-called Meyer–Miller (MM) classical electron analog model. In the Cartesian version of the MM-representation, the Hamiltonian for an  $n$ -state problem is the following harmonic oscillator Hamiltonian,<sup>13,14,9d,31</sup>

$$\begin{aligned} H(\mathbf{x}, \mathbf{p}) &= \sum_{k=1}^n \frac{1}{2} (x_k^2 + p_k^2 - 1) H_{kk} \\ &\quad + \sum_{k=1}^n \sum_{l=k+1}^n H_{k,l} (x_k x_l + p_k p_l), \end{aligned} \quad (2.9)$$

where  $H_{kk}$  and  $H_{kl}$  are the diagonal and off-diagonal matrix elements which define the discrete Hamiltonian. Since the total number of quanta of excitation in this system of  $n$  harmonic oscillators is a constant of the motion, the  $n$  ‘‘electronic’’ states that correspond to one quantum of excitation in one of the modes and no quanta in all the others, form a complete set within this subspace. The ‘‘electronic’’ wave functions for these  $n$  states are thus given by ( $m = \omega = \hbar = 1$ )

$$\Phi_k(\mathbf{x}) = \phi_1(x_k) \prod_{l=1, l \neq k}^n \phi_0(x_l), \quad (2.10a)$$

where

$$\phi_0(x) = \frac{1}{\pi^{1/4}} e^{-x^2/2}, \quad (2.10b)$$

$$\phi_1(x) = \frac{\sqrt{2}}{\pi^{1/4}} x e^{-x^2/2}. \quad (2.10c)$$

It is easily verified that  $\{H_{kk'}\}$ , the matrix of the MM-Hamiltonian, Eq. (2.9) in the  $n$ -dimensional basis of Eq. (2.10), is precisely the original diabatic electronic matrix.

Applying Eq. (2.9) to Eq. (1.1) yields the continuous MM-representation for the spin-boson problem

$$H(\mathbf{x}, \mathbf{p}, \mathbf{Q}, \mathbf{P}) = \Delta(p_1 p_2 + x_1 x_2) + (h_1 + h_2)H_B + (h_2 - h_1)H_c, \quad (2.11a)$$

where

$$h_1 = \frac{1}{2}(p_1^2 + x_1^2 - 1), \quad h_2 = \frac{1}{2}(p_2^2 + x_2^2 - 1), \quad (2.11b)$$

and the wave functions for the two diabatic states are

$$\Phi_1(x_1, x_2) = \phi_1(x_1)\phi_0(x_2), \quad \Phi_2(x_1, x_2) = \phi_0(x_1)\phi_1(x_2). \quad (2.12)$$

It is then straightforward to apply the LSC-IVR formalism to the spin-boson problem.

In this paper, two correlation functions are used to study the dynamics of the spin-boson problem. For the purpose of studying the time evolution of the density matrix and its coherent to incoherent transition, we evaluate the population-spin correlation function  $P(t)$ , defined as<sup>17</sup>

$$P(t) = \frac{1}{Q_B} \text{tr}[\hat{\rho}_{11} e^{\beta \hat{H}_B} e^{i\hat{H}t/\hbar} \hat{\sigma}_z e^{-i\hat{H}t/\hbar}] \\ \equiv P_{1 \leftarrow 1}(t) - P_{2 \leftarrow 1}(t), \quad (2.13)$$

where

$$\hat{\rho}_{11} = |\Phi_1\rangle\langle\Phi_1|, \quad (2.14a)$$

$$\hat{\sigma}_z = |\Phi_1\rangle\langle\Phi_1| - |\Phi_2\rangle\langle\Phi_2|, \quad (2.14b)$$

$$Q_B = \text{tr}[e^{-\beta \hat{H}_B}]. \quad (2.14c)$$

The assumption in evaluating  $P(t)$  is that the interaction between the system and the bath is switched on at  $t=0$ , and the initial population is on state 1, i.e., the initial density matrix is

$$\hat{\rho}(0) = \hat{\rho}_{11} e^{-\beta \hat{H}_B}. \quad (2.15)$$

$P(t)$  is thus unity at  $t=0$  [since  $P_{1 \leftarrow 1}(0) = 1$  and  $P_{2 \leftarrow 1}(0) = 0$ ] and decays to zero in the presence of a finite electronic-nuclear coupling since the two degenerate electronic states have equal population at equilibrium ( $t \rightarrow \infty$ ). It is easy to apply the general LSC-IVR result of Eq. (2.6) to express  $P(t)$  as follows:

$$P(t) = \frac{1}{(2\pi\hbar)^{N+2} Q_B} \int d\mathbf{Q}_0 \int d\mathbf{P}_0 \\ \times \int d\mathbf{x}_0 \int d\mathbf{p}_0 \rho_{11}^w(\mathbf{x}_0, \mathbf{p}_0) \rho_B^w(\mathbf{Q}_0, \mathbf{P}_0) \sigma_z^w(\mathbf{x}_t, \mathbf{p}_t), \quad (2.16)$$

where  $\rho_B^w(\mathbf{Q}_0, \mathbf{P}_0)$  is the Wigner transform of  $e^{-\beta \hat{H}_B}$ , and  $N$  the number of bath degrees of freedom.

For the purpose of calculating the rate constant, we found it most convenient to apply the flux correlation function formalism.<sup>32,33</sup> Thus, the thermal rate constant is expressed via a flux-side correlation function,<sup>32b</sup>

$$k(T) = Q_r(T)^{-1} \lim_{t \rightarrow t_p} C_{fs}(t), \quad (2.17)$$

where  $t_p$  is the ‘‘plateau’’ time, and

$$C_{fs}(t) = \text{tr}[\hat{F}(\beta) e^{i\hat{H}t/\hbar} \hat{h} e^{-i\hat{H}t/\hbar}], \quad (2.18)$$

$\hat{F}(\beta)$  is the Boltzmannized flux operator

$$\hat{F}(\beta) = e^{-\beta \hat{H}/2} \hat{F} e^{-\beta \hat{H}/2}, \quad (2.19a)$$

$$\hat{F} = \frac{i}{\hbar} [\hat{H}, \hat{h}], \quad (2.19b)$$

and  $\hat{h}$  is the operator that projects the wave function to the product side. Similar to the above analysis of the population-spin correlation function  $P(t)$ , the LSC-IVR approximation for the flux-side correlation function  $C_{fs}(t)$  is given by

$$C_{fs}(t) = (2\pi\hbar)^{-N-2} \int d\mathbf{Q}_0 \int d\mathbf{P}_0 \\ \times \int d\mathbf{x}_0 \int d\mathbf{p}_0 F_\beta^w(\mathbf{x}_0, \mathbf{p}_0; \mathbf{Q}_0, \mathbf{P}_0) h^w(\mathbf{x}_t, \mathbf{p}_t, \mathbf{Q}_t, \mathbf{P}_t). \quad (2.20)$$

If the reaction is adiabatic (i.e., occurs on a single electronic potential surface), the thermal rate constant of Eq. (2.17) has a similar LSC-IVR expression for the flux-side correlation function

$$C_{fs}(t) = (2\pi\hbar)^{-f} \int d\mathbf{q}_0 \int d\mathbf{p}_0 F_\beta^w(\mathbf{q}_0, \mathbf{p}_0) h^w(\mathbf{q}_t, \mathbf{p}_t), \quad (2.21)$$

where  $f$  is number of degrees of freedom for the molecular system and  $(\mathbf{q}, \mathbf{p})$  are the phase space variables. In previous work,<sup>11</sup> the projection operator  $\hat{h}$  is chosen as the step function of the reaction coordinate  $s$ ,  $\hat{h} = \hat{h}[s(\mathbf{q})]$ , where  $s(\mathbf{q})$  is some function of the coordinates  $\mathbf{q}$  that is positive (negative) on the product (reactant) side of the dividing surface. It is easy to see that the Wigner transform  $h^w(\mathbf{q}_t, \mathbf{p}_t)$  is simply the step function of the reaction coordinate

$$h^w(\mathbf{q}_t, \mathbf{p}_t) = h[s(\mathbf{q}_t)], \quad (2.22)$$

and Eq. (2.21) reduces to

$$C_{fs}(t) = (2\pi\hbar)^{-f} \int d\mathbf{q}_0 \int d\mathbf{p}_0 F_\beta^w(\mathbf{q}_0, \mathbf{p}_0) h[s(\mathbf{q}_t)], \quad (2.23)$$

which is Eq. (3.14) of Ref. 11 if the factor  $(2\pi\hbar)^{-f}$  is merged into the Wigner distribution function  $F_\beta^w(\mathbf{q}_0, \mathbf{p}_0)$ .

### III. DETAILS OF THE CALCULATION

#### A. Bath discretization

To treat the continuum of harmonic bath modes we introduce a density of frequencies  $\rho(\omega)$  and discretize the continuum of frequencies as follows:

$$\int_0^{\omega_j} d\omega \rho(\omega) = j, \quad j = 1, \dots, N. \quad (3.1a)$$

The coupling constant  $c_j$  for each frequency  $\omega_j$  is then given by

$$c_j^2 = \omega_j \frac{2 J_D(\omega_j)}{\pi \rho(\omega_j)} \quad (3.1b)$$

The precise functional form of  $\rho(\omega)$  does not affect the final answer if enough bath modes are included, but it does affect the efficiency in solving the problem. This is particularly true for the Debye spectral density since it covers such a broad frequency range. We have found that choosing the density of frequencies as

$$\rho(\omega) = \frac{N}{2\sqrt{\omega\omega_{\max}}}, \quad (3.2)$$

gives satisfactory description of the bath with 1000 bath modes. The discrete frequencies, according to Eqs. (3.1a) and (3.2), are

$$\omega_j = \frac{j^2}{N^2} \omega_{\max}, \quad j = 1, \dots, N, \quad (3.3)$$

and the system-bath coupling  $c_j$  is calculated from Eq. (3.1b). The maximum frequency  $\omega_{\max}$  is set to be 20–200 $\omega_c$  depending on specific parameters in the simulation. In any case, the reorganization energy

$$E_r = 2\eta \approx 2 \sum_j^N \frac{c_j^2}{\omega_j^2} \quad (3.4)$$

was accurately reproduced.

It should be clear that nothing in our approach takes any explicit advantage of the fact that the bath is harmonic and that the coupling is linear (as is necessary, for example, in quantum path integral calculations<sup>19,20</sup>). It would thus be possible to carry out the present LSC-IVR calculations for anharmonic baths and nonlinear coupling with essentially no increase in effort.

## B. The Wigner distribution functions

The Wigner transform of the various operators defined in Sec. II can be obtained via straightforward integration, for which we will give the final expressions and leave the details to the reader (hereafter  $\hbar = 1$ ). For the population-spin correlation function  $P(t)$ , Eq. (2.16), the Wigner distribution functions are

$$\begin{aligned} \rho_{11}^w(\mathbf{x}_0, \mathbf{p}_0) &= \int d\Delta \mathbf{x} e^{-i\mathbf{p}_0 \cdot \Delta \mathbf{x}} \left\langle \mathbf{x}_0 + \frac{\Delta \mathbf{x}}{2} \left| \hat{\rho}_{11} \right| \mathbf{x}_0 - \frac{\Delta \mathbf{x}}{2} \right\rangle \\ &= 8(x_{10}^2 + p_{10}^2 - \frac{1}{2}) e^{-(x_{10}^2 + p_{10}^2)} e^{-(x_{20}^2 + p_{20}^2)}, \end{aligned} \quad (3.5a)$$

$$\begin{aligned} \rho_B^w(\mathbf{Q}_0, \mathbf{P}_0) &= \int d\Delta \mathbf{Q} e^{-i\mathbf{P}_0 \cdot \Delta \mathbf{Q}} \left\langle \mathbf{Q}_0 + \frac{\Delta \mathbf{Q}}{2} \left| e^{-\beta \hat{H}_B} \right| \mathbf{Q}_0 - \frac{\Delta \mathbf{Q}}{2} \right\rangle \\ &= \prod_j^N \frac{1}{\cosh(\beta \omega_j/2)} \\ &\quad \times \exp \left[ -\frac{2 \tanh(\beta \omega_j/2)}{\omega_j} \left( \frac{P_{j0}^2}{2} + \frac{1}{2} \omega_j^2 Q_{j0}^2 \right) \right], \end{aligned} \quad (3.5b)$$

$$\begin{aligned} \sigma_z^w(\mathbf{x}_t, \mathbf{p}_t) &= \int d\Delta \mathbf{x} e^{-i\mathbf{p}_t \cdot \Delta \mathbf{x}} \left\langle \mathbf{x}_t + \frac{\Delta \mathbf{x}}{2} \left| \hat{\sigma}_z \right| \mathbf{x}_t - \frac{\Delta \mathbf{x}}{2} \right\rangle \\ &= 8(x_{1t}^2 + p_{1t}^2 - x_{2t}^2 - p_{2t}^2) e^{-(x_{1t}^2 + p_{1t}^2)} e^{-(x_{2t}^2 + p_{2t}^2)}. \end{aligned} \quad (3.5c)$$

For the flux-side correlation function  $C_{fs}(t)$  in Eq. (2.18), the projection operator  $\hat{h}$  is naturally defined as

$$\hat{h} = \hat{\rho}_{22} = |\Phi_2\rangle\langle\Phi_2| \quad (3.6)$$

(i.e., it projects wave functions onto state 2), and the resulting flux operator is

$$\hat{F} = i[\hat{H}, \hat{h}] = i\Delta(|\Phi_1\rangle\langle\Phi_2| - |\Phi_2\rangle\langle\Phi_1|). \quad (3.7)$$

The Wigner distribution function for the projection operator in Eq. (2.20) is simply

$$\begin{aligned} h^w(\mathbf{x}_t, \mathbf{p}_t) &= \int d\Delta \mathbf{x} e^{-i\mathbf{p}_t \cdot \Delta \mathbf{x}} \left\langle \mathbf{x}_t + \frac{\Delta \mathbf{x}}{2} \left| \hat{h} \right| \mathbf{x}_t - \frac{\Delta \mathbf{x}}{2} \right\rangle \\ &= 8(x_{2t}^2 + p_{2t}^2 - \frac{1}{2}) e^{-(x_{1t}^2 + p_{1t}^2)} e^{-(x_{2t}^2 + p_{2t}^2)}. \end{aligned} \quad (3.8)$$

There is, however, no analytic result for the Wigner transform of the Boltzmannized flux operator,  $\hat{F}(\beta)$  in Eq. (2.19a). The simplest approximation, similar to the assumption in defining the population-spin correlation function  $P(t)$ , is

$$\hat{F}(\beta) = e^{-\beta \hat{H}/2} \hat{F} e^{-\beta \hat{H}/2} \approx [e^{-\beta \hat{H}_s/2} \hat{F} e^{-\beta \hat{H}_s/2}] e^{-\beta \hat{H}_B}, \quad (3.9)$$

where we denote the ‘‘system’’ Hamiltonian as

$$\hat{H}_s = \Delta(|\Phi_1\rangle\langle\Phi_2| + |\Phi_2\rangle\langle\Phi_1|), \quad (3.10)$$

and it is easy to verify that

$$e^{-\beta \hat{H}_s/2} \hat{F} e^{-\beta \hat{H}_s/2} = \hat{F}, \quad (3.11)$$

so that Eq. (3.9) reduces to

$$\hat{F}(\beta) = \hat{F} e^{-\beta \hat{H}_B}. \quad (3.12)$$

Thus the Wigner distribution function for  $\hat{F}(\beta)$  is

$$F_\beta^w(\mathbf{x}_0, \mathbf{p}_0; \mathbf{Q}_0, \mathbf{P}_0) = F^w(\mathbf{x}_0, \mathbf{p}_0) \rho_B^w(\mathbf{Q}_0, \mathbf{P}_0), \quad (3.13a)$$

where  $\rho_B^w(\mathbf{Q}_0, \mathbf{P}_0)$  is given in Eq. (3.5b), and

$$\begin{aligned} F^w(\mathbf{x}_0, \mathbf{p}_0) &= \int d\Delta \mathbf{x} e^{-i\mathbf{p}_0 \cdot \Delta \mathbf{x}} \left\langle \mathbf{x}_0 + \frac{\Delta \mathbf{x}}{2} \left| \hat{F} \right| \mathbf{x}_0 - \frac{\Delta \mathbf{x}}{2} \right\rangle \\ &= 16\Delta(x_{20}p_{10} - x_{10}p_{20}) e^{-(x_{10}^2 + p_{10}^2)} e^{-(x_{20}^2 + p_{20}^2)}. \end{aligned} \quad (3.13b)$$

A better approximation is based on the split-operator approach of the Boltzmann operator

$$e^{-\beta \hat{H}/2} \approx e^{-\beta \hat{H}_s/4} e^{-\beta \hat{H}_B/2} e^{-\beta \hat{H}_s/4}, \quad (3.14a)$$

where we have denoted

$$\hat{H}_{Bc} = \begin{bmatrix} H_B - H_c & 0 \\ 0 & H_B + H_c \end{bmatrix} = (H_B - H_c)|\Phi_1\rangle\langle\Phi_1| + (H_B + H_c)|\Phi_2\rangle\langle\Phi_2|. \quad (3.14b)$$

After some manipulations, we arrive at the final form of the Wigner distribution function for  $\hat{F}(\beta)$

$$F_\beta^w(\mathbf{x}_0, \mathbf{p}_0; \mathbf{Q}_0, \mathbf{P}_0) = G^w(\mathbf{x}_0, \mathbf{p}_0; \mathbf{Q}_0, \mathbf{P}_0) Z^w(\mathbf{x}_0, \mathbf{p}_0; \mathbf{Q}_0, \mathbf{P}_0), \quad (3.15a)$$

$$G^w(\mathbf{x}_0, \mathbf{p}_0; \mathbf{Q}_0, \mathbf{P}_0) = 16\Delta e^{-(x_{10}^2 + p_{10}^2 + x_{20}^2 + p_{20}^2)} \times \prod_j \frac{1}{\cosh(u_j)} e^{-\tanh(u_j)(P_{j0}^2 + \omega_j^2 Q_{j0}^2)/\omega_j}, \quad (3.15b)$$

$$Z^w(\mathbf{x}_0, \mathbf{p}_0; \mathbf{Q}_0, \mathbf{P}_0) = A^w(\mathbf{P}_0) \left[ \sinh\left(\frac{\beta\Delta}{2}\right) B^w(\mathbf{x}_0, \mathbf{p}_0) - \cosh\left(\frac{\beta\Delta}{2}\right) C^w(\mathbf{x}_0, \mathbf{p}_0) \right] + D^w(\mathbf{P}_0) E^w(\mathbf{x}_0, \mathbf{p}_0), \quad (3.15c)$$

$$A^w(\mathbf{P}_0) = - \left\{ \prod_j e^{[c_j^2/(2\omega_j^2)][\beta - 2 \tanh(u_j)/\omega_j]} \right\} \times \sin \left\{ \sum_j \left[ \frac{1}{\cosh(u_j)} - 1 \right] \frac{2c_j}{\omega_j^2} P_{j0} \right\}, \quad (3.15d)$$

$$B^w(\mathbf{x}_0, \mathbf{p}_0) = \frac{1}{2}(x_{10}^2 + p_{10}^2 + x_{20}^2 + p_{20}^2 - 1), \quad (3.15e)$$

$$C^w(\mathbf{x}_0, \mathbf{p}_0) = x_{10}x_{20} + p_{10}p_{20}, \quad (3.15f)$$

$$D^w(\mathbf{P}_0) = \left\{ \prod_j e^{[c_j^2/(2\omega_j^2)][\beta - 2 \tanh(u_j)/\omega_j]} \right\} \times \cos \left\{ \sum_j \left[ \frac{1}{\cosh(u_j)} - 1 \right] \frac{2c_j}{\omega_j^2} P_{j0} \right\}, \quad (3.15g)$$

$$E^w(\mathbf{x}_0, \mathbf{p}_0) = x_{20}p_{10} - x_{10}p_{20}, \quad (3.15h)$$

and

$$u_j = \beta\omega_j/2. \quad (3.15i)$$

It should be emphasized that the Wigner distribution function for the Boltzmannized flux operator,  $F_\beta^w(\mathbf{x}_0, \mathbf{p}_0; \mathbf{Q}_0, \mathbf{P}_0)$ , is only used for weighting initial conditions of classical trajectories; the real time dynamics is still solved with the full Hamiltonian. The above approximations for  $F_\beta^w(\mathbf{x}_0, \mathbf{p}_0; \mathbf{Q}_0, \mathbf{P}_0)$  are satisfactory for cases considered in this paper. There are of course more accurate methods (e.g., see Ref. 35) of evaluating  $F_\beta^w(\mathbf{x}_0, \mathbf{p}_0; \mathbf{Q}_0, \mathbf{P}_0)$  or equivalently, the overall partition function for the spin-boson system, which should be incorporated for calculations that consider lower temperatures than treated herein.

### C. Equations of motion

Hamilton's equations of motion for the MM-representation of the spin-boson problem, Eq. (2.11), are straightforward

$$\dot{x}_1 = \frac{\partial H}{\partial p_1} = p_1(H_B - H_c) + p_2\Delta, \quad (3.16a)$$

$$\dot{p}_1 = -\frac{\partial H}{\partial x_1} = -x_1(H_B - H_c) - x_2\Delta, \quad (3.16b)$$

$$\dot{x}_2 = \frac{\partial H}{\partial p_2} = p_1\Delta + p_2(H_B + H_c), \quad (3.16c)$$

$$\dot{p}_2 = -\frac{\partial H}{\partial x_2} = -x_1\Delta - x_2(H_B + H_c), \quad (3.16d)$$

$$\dot{Q}_j = \frac{\partial H}{\partial P_j} = P_j(h_1 + h_2), \quad (3.16e)$$

$$\dot{P}_j = -\frac{\partial H}{\partial Q_j} = -\omega_j^2 Q_j(h_1 + h_2) - c_j(h_2 - h_1). \quad (3.16f)$$

Unfortunately, one encounters numerical problems when directly integrating the above equations because the term  $H_B = \sum_j \frac{1}{2}(P_j^2 + \omega_j^2 Q_j^2)$  has a large magnitude in Eqs. (3.16a)–(3.16d), and this gives rise to rapid changes in the variables  $\{x_1, p_1, x_2, p_2\}$  versus time. As a result, Eqs. (3.16) are a stiff set of equations.

This problem can be resolved by changing the integration variables from  $\{x_1, p_1, x_2, p_2\}$  to  $\{h_1 + h_2, h_1 - h_2, p_2x_1 - p_1x_2, p_1p_2 + x_1x_2\}$ . Equations (3.16(a)–(3.16d) are then replaced by the following equivalent set of equations:

$$\frac{d}{dt}(h_1 + h_2) = 0, \quad (3.17a)$$

$$\frac{d}{dt}(h_1 - h_2) = 2\Delta(p_2x_1 - p_1x_2), \quad (3.17b)$$

$$\frac{d}{dt}(p_2x_1 - p_1x_2) = -2\Delta(h_1 - h_2) - 2H_c(p_1p_2 + x_1x_2), \quad (3.17c)$$

$$\frac{d}{dt}(p_1p_2 + x_1x_2) = 2H_c(p_2x_1 - p_1x_2). \quad (3.17d)$$

Equations (3.17) not only solve the stiff equation problem (the term  $H_B$  is no longer present!), but also closely relate the integration variables to physical quantities:  $h_1 + h_2$  represents the total population in the two states, which is obviously a conserved quantity [as seen from Eq. (3.17a)];  $h_1 - h_2$  represents population difference between state 1 and 2;  $p_2x_1 - p_1x_2$  relates to the flux from one state to another; and  $p_1p_2 + x_1x_2$  represents the off-diagonal terms in the MM-Hamiltonian.

### IV. RESULTS AND DISCUSSION

Before considering application of the LSC-IVR to the spin-boson problem of Eq. (1.1), it is of pedagogical interest to show how it applies to the isolated two level system,

$$\hat{H} = \begin{bmatrix} \epsilon & \Delta \\ \Delta & -\epsilon \end{bmatrix}; \quad (4.1)$$

we thus remove the bath from the spin-boson Hamiltonian, Eq. (1.1), and set  $\epsilon \neq 0$  as the bias to differentiate the energy levels of the two states. This is a similar case to the previous study<sup>21</sup> of a one-dimensional double well problem, where the correlation functions display coherent oscillations between reactants and products.

The Meyer–Miller representation for Eq. (4.1) is

$$H = \frac{\epsilon}{2}(p_1^2 + x_1^2 - p_2^2 - x_2^2) + \Delta(p_1 p_2 + x_1 x_2), \quad (4.2)$$

and we consider, for example, the population-spin correlation function

$$P(t) = \text{tr}[\hat{\rho}_{11} e^{i\hat{H}t} \hat{\sigma}_z e^{-i\hat{H}t}], \quad (4.3)$$

via the LSC-IVR approximation,

$$P(t) = \frac{1}{(2\pi)^2} \int dx_{10} \int dp_{10} \int dx_{20} \int dp_{20} \times \rho_{11}^w(x_{10}, p_{10}, x_{20}, p_{20}) \sigma_z^w(x_{1t}, p_{1t}, x_{2t}, p_{2t}), \quad (4.4)$$

where  $\rho_{11}^w$  and  $\sigma_z^w$  are given in Eqs. (3.5a) and (3.5c), respectively. Hamilton's equations of motion for Eq. (4.2) are solvable:

$$x_{1t} = \cos(\sqrt{\epsilon^2 + \Delta^2}t)x_{10} + \frac{\sin(\sqrt{\epsilon^2 + \Delta^2}t)}{\sqrt{\epsilon^2 + \Delta^2}}(p_{10}\epsilon + p_{20}\Delta), \quad (4.5a)$$

$$p_{1t} = \cos(\sqrt{\epsilon^2 + \Delta^2}t)p_{10} - \frac{\sin(\sqrt{\epsilon^2 + \Delta^2}t)}{\sqrt{\epsilon^2 + \Delta^2}}(x_{10}\epsilon + x_{20}\Delta), \quad (4.5b)$$

$$x_{2t} = \cos(\sqrt{\epsilon^2 + \Delta^2}t)x_{20} + \frac{\sin(\sqrt{\epsilon^2 + \Delta^2}t)}{\sqrt{\epsilon^2 + \Delta^2}}(-p_{20}\epsilon + p_{10}\Delta), \quad (4.5c)$$

$$p_{2t} = \cos(\sqrt{\epsilon^2 + \Delta^2}t)p_{20} + \frac{\sin(\sqrt{\epsilon^2 + \Delta^2}t)}{\sqrt{\epsilon^2 + \Delta^2}}(x_{20}\epsilon - x_{10}\Delta). \quad (4.5d)$$

Using Eqs. (4.5), the phase space integration in Eq. (4.4) can now be carried out over the initial condition variables  $(x_{10}, p_{10}, x_{20}, p_{20})$  to give

$$P(t) = 1 - \frac{2\Delta^2 \sin^2(\sqrt{\epsilon^2 + \Delta^2}t)}{\epsilon^2 + \Delta^2}, \quad (4.6)$$

which is recognized to be the exact quantum mechanical result.

Equation (4.6) is the result of the spin-boson problem [Eq. (1.1)] when the system-bath coupling  $H_c$  is zero (with the trivial modification  $\epsilon = 0$ ). In this case, the population-spin correlation function  $P(t)$  exhibits pure coherent motions between the two states, and the rate constant from state 1 to 2 is not defined. As the coupling increases,  $P(t)$  will undergo a coherent to incoherent transition and may eventually reach the form of an exponential decay for which a rate

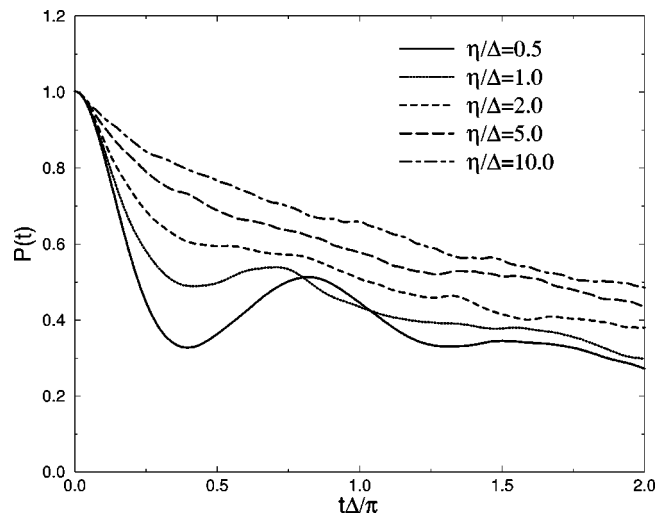


FIG. 2. Coherent–incoherent transition vs  $\eta$ :  $P(t)$  for  $\beta\Delta = 0.1$  and  $\omega_c/\Delta = 0.25$ .

constant can be defined. It is possible that other parameters also play important roles in the coherent to incoherent transition. Below, we will discuss such behavior in the complete parameter space.

## A. Coherent to incoherent transitions

### 1. Along the $\eta$ -axis

This is the most obvious axis for observing the transition from coherent to incoherent behavior. The parameter  $\eta$  measures the coupling strength between the bath and the two level system (also recall that  $2\eta$  is the reorganization energy). Therefore as  $\eta$  increases, the energy exchange between the system and the bath becomes more efficient so that the bath more effectively damps the coherent motion of the two level system. Figure 2 shows the population-spin correlation function,  $P(t)$ , for the parameters  $\beta\Delta = 0.1$  and  $\omega_c/\Delta = 0.25$ . As seen clearly in the figure, there are strong coherent features for the weak coupling case of  $\eta/\Delta = 0.5$ , less so for a stronger coupling  $\eta = 1$ . It reaches the transition boundary between  $\eta/\Delta = 2$  and  $\eta/\Delta = 5$ , and one sees no remaining coherent features for the strong coupling case of  $\eta/\Delta = 10$ . It should be pointed out that although  $\eta/\Delta = 10$  displays totally incoherent dynamics, it does not give the golden rule rate constant for the parameters used in Fig. 2. Rather, it gives a rate that agrees with Zusman's solvent dynamical model.<sup>34</sup> Such results will be discussed more fully below.

### 2. Along the $T$ -axis

This is also an interesting parameter for observing the coherent to incoherent transition. At low temperature, the total number of states accessible for the bath is limited and so is energy exchange between the system and the bath. As the temperature increases, more bath states participate in the energy transfer process, which tends to destroy the coherent motion of the two level system. Figure 3 shows  $P(t)$  for different temperatures (here we use  $\beta\Delta$  as a measure of temperature). The other parameters are  $\eta/\Delta = 2.0$  and  $\omega_c/\Delta$

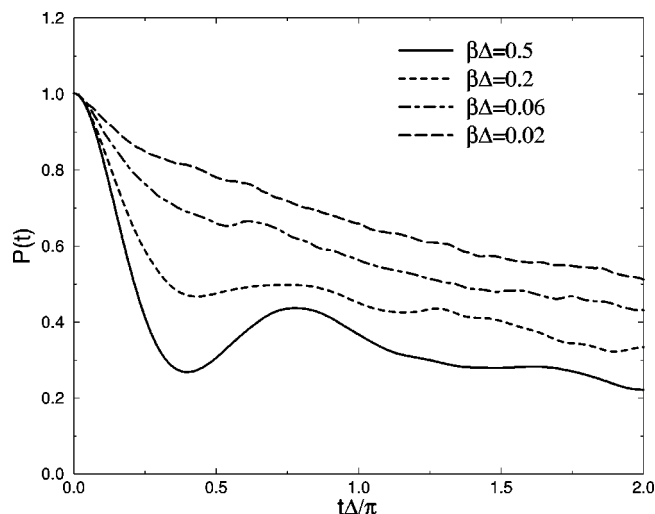


FIG. 3. Coherent–incoherent transition vs  $T$ :  $P(t)$  for  $\eta/\Delta=0.1$  and  $\omega_c/\Delta=0.25$ .

$=0.25$ . At low temperature,  $\beta\Delta=0.5$ , there is strong coherent character in  $P(t)$ . The coherent component becomes less for a higher temperature of  $\beta\Delta=0.2$ , and there is barely any coherence left for the still higher temperature of  $\beta\Delta=0.06$ . At the highest temperature in Fig. 3,  $\beta\Delta=0.02$ ,  $P(t)$  displays totally incoherent dynamics.

### 3. Along the $\omega_c$ -axis

This is a less obvious axis for observing the coherent to incoherent transition, but the most interesting one. For reasons which become clear below, the  $\omega_c$ -axis covers several important dynamic aspects and is crucial for both identifying the coherent–incoherent transition and calculating the rate constant. Figure 4 shows  $P(t)$  at  $\beta\Delta=0.5$  and  $\eta/\Delta=20.0$ , for several  $\omega_c$ 's. The trend is very clear: for the smallest  $\omega_c$  in the figure,  $\omega_c/\Delta=0.025$ ,  $P(t)$  shows strongly coherent character. The coherence becomes less prominent as  $\omega_c/\Delta$  is

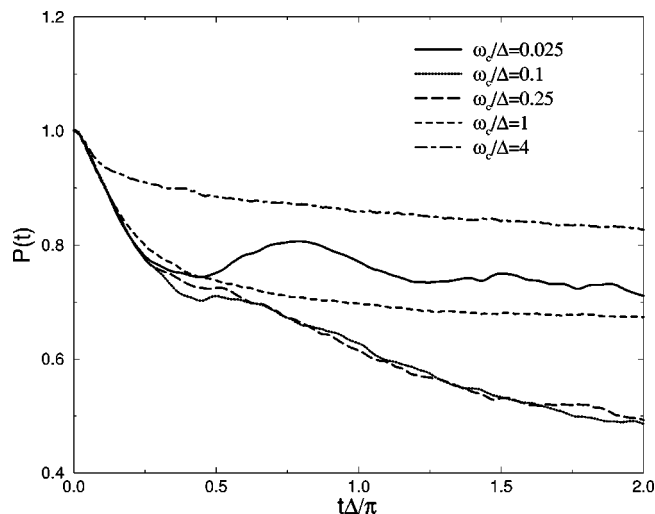


FIG. 4. Coherent–incoherent transition vs  $\omega_c$ :  $P(t)$  for  $\eta/\Delta=20$  and  $\beta\Delta=0.5$ .

increased to 0.1, and has almost disappeared for  $\omega_c/\Delta=0.25$ . For  $\omega_c/\Delta=4$ ,  $P(t)$  exhibits complete incoherent dynamics.

It is more illustrative to look at the flux-side correlation function,  $C_{fs}(t)$ , for the above cases, especially from  $\omega_c/\Delta=0.1$  to  $\omega_c/\Delta=1$  where the coherent to incoherent transition is not so obvious. Figure 5(a) shows  $C_{fs}(t)$  for the case  $\omega_c/\Delta=0.1$  in Fig. 4. (The correlation function was multiplied by the factor  $Q_r e^{\beta E_a/\Delta}$ , where

$$Q_r = \text{tr}[\Phi_1] \langle \Phi_1 | e^{-\beta(\hat{H}_B - \hat{H}_c)} | \Phi_1 \rangle = Q_B \exp \left[ \beta \sum_j \frac{c_j^2}{2\omega_j^2} \right], \quad (4.7a)$$

is the reactant's partition function with  $Q_B$  the partition function for the harmonic bath, and

$$\sum_j \frac{c_j^2}{2\omega_j^2} = \frac{\eta}{2} = E_a, \quad (4.7b)$$

is the usual activation energy in the infinite bath limit.) Because  $C_{fs}(t)$  is an odd function of time, it starts from zero at  $t=0$ , and quickly reaches its maximum by a time of  $\sim \beta\hbar$  ( $\beta\Delta$  in terms of the units here).<sup>32</sup> After that, it is seen that the flux displays sizable coherent recrossings of the dividing surface. One can see from the second to the third peak that the period of oscillation agrees approximately with the Rabi period in Eq. (4.6). On the other hand, Fig. 5(b) shows  $C_{fs}(t)$  for a larger characteristic frequency, i.e. the  $\omega_c/\Delta=0.25$  case in Fig. 4, and it is seen that the coherence feature is mostly quenched by the bath. At longer time,  $C_{fs}(t)$  reaches a plateau corresponding to a rate constant that is significantly smaller than the golden-rule prediction, but agrees very well with Zusman's model.<sup>34</sup> Figure 5(c) shows  $C_{fs}(t)$  for an even larger  $\omega_c$  ( $\omega_c/\Delta=1$ ), and here it is clear that the dynamics is incoherent. Again, there are recrossings of the dividing surface and the rate constant agrees with Zusman's model<sup>34</sup> instead of the golden-rule result. Finally, Fig. 5(d) shows  $C_{fs}(t)$  for the largest characteristic frequency in Fig. 4,  $\omega_c/\Delta=4$ , and it is a classic example of a "direct" reaction<sup>36</sup> where no hint of recrossing is present. Naturally, the rate constant in this case agrees very well with the golden-rule prediction.

Thus, the physics along the  $\omega_c$ -axis is as follows: when  $\omega_c$  starts from zero and gradually increases, the relaxation of the bath is extremely slow, unable to destroy the coherent motion of the two level system. As  $\omega_c$  becomes larger, the response of bath becomes faster so that the bath gradually participates in the decoherence mechanism. The first incoherence regime appears, however, still at quite small  $\omega_c$ . This is the regime where the collective bath motion is slower or at least at the same timescale of the two level system. As a result, the slow diffusive motion of the bath manifest itself into the overall dynamics, a phenomenon observed from experiment<sup>37</sup> and theoretically predicted by Zusman nearly two decades ago.<sup>34</sup> When  $\omega_c$  is large enough, the timescale separation between the bath and the two level system is large enough for the dynamics to become transition state theory-like and well described by the golden-rule.



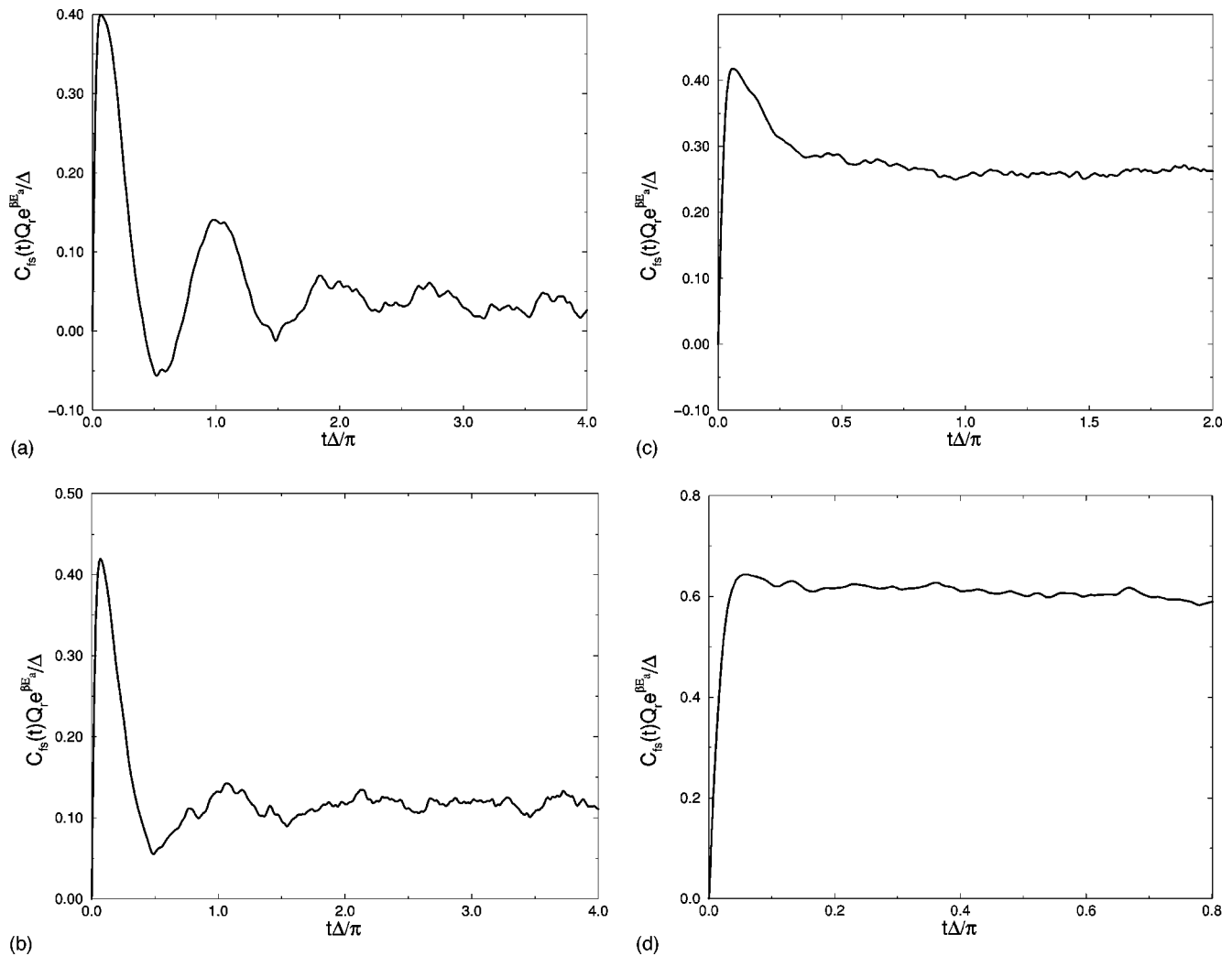


FIG. 5. Flux-side correlation function  $C_{fs}(t)$  for  $\beta\Delta=0.5$  and  $\eta/\Delta=20$ , and the characteristic frequency  $\omega_c$  is: (a)  $\omega_c/\Delta=0.1$ ; (b)  $\omega_c/\Delta=0.25$ ; (c)  $\omega_c/\Delta=1$ ; and (d)  $\omega_c/\Delta=4$ .

#### 4. Comparison with the noninteracting-blip approximation

The so-called noninteracting-blip approximation (NIBA)<sup>17</sup> is a useful approximation in studying the spin-boson problem. It gives the correct limit for both the extreme weak coupling regime (coherence) and the golden-rule regime (incoherence). Based on this, it is argued<sup>17</sup> that (for the Ohmic spectral density in particular) NIBA may give qualitatively correct description of spin-boson dynamics over a broad parameter space. For an Ohmic spectral density with an exponential cutoff, it is indeed found from Monte Carlo path integral simulations<sup>20</sup> and LSC-IVR calculation<sup>12</sup> that the NIBA gives correct results for several choices of parameters and predicts correctly the coherent–incoherent transition.

A different situation is expected for the Debye spectral density due to its much broader spectral range. The above two limiting cases should still hold, but the transition regime may be more complicated. For example, it is known that NIBA, bearing the spirit of the first-order perturbation theory,<sup>38</sup> cannot describe Zusman-type dynamics of Fig. 4 and Fig. 5(b) and 5(c). It is also reasonable to believe that

NIBA will fail to describe recrossing dynamics from any other causes.

Figure 6 compares LSC-IVR results with NIBA for three different couplings ( $\eta$ ). The other two parameters used in the calculation are  $\beta\Delta=0.5$  and  $\omega_c/\Delta=10$ . For the smallest coupling in the figure,  $\eta/\Delta=0.1$ , both LSC-IVR and NIBA predict coherent dynamics, and they agree well with each other. On the other hand, both LSC-IVR and NIBA predict incoherent dynamics for the largest coupling in Fig. 6,  $\eta/\Delta=20$ , and the fitted rates agree well with the golden-rule prediction. The problem occurs for the intermediate coupling,  $\eta/\Delta=1$ , where NIBA predicts coherent dynamics but LSC-IVR predicts, after a short transient time, incoherent relaxation.

Again, we seek the help from the flux-side correlation function,  $C_{fs}(t)$ . Figure 7 shows  $C_{fs}(t)$  for the  $\eta/\Delta=1$  case of Fig. 6, and it becomes immediately apparent that there is significant recrossing dynamics (in fact it is in the so-called energy-diffusion regime): by  $t\Delta \approx \beta\Delta C_{fs}(t)$  has reached its maximum, but the coupling to the bath is not strong enough to prevent flux from recrossing the dividing surface. At longer time, a plateau is reached that gives a rate constant

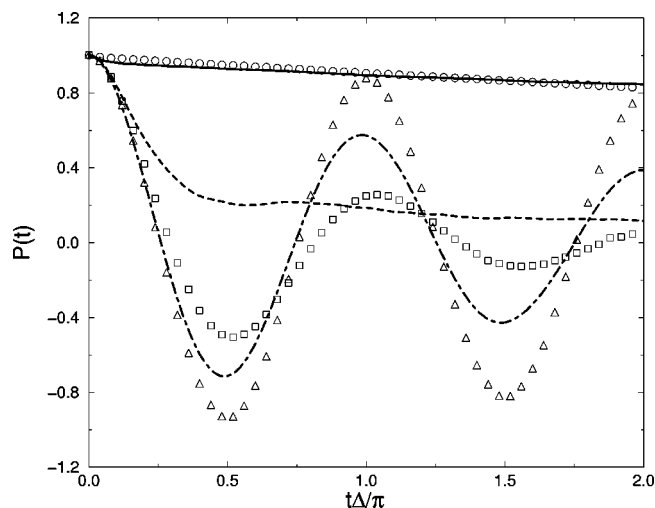


FIG. 6. Comparison of the LSC-IVR simulation with the NIBA result: The solid line and the open circle correspond to the LSC-IVR and NIBA result for  $\eta/\Delta=20$ , respectively; the dashed line and the square correspond to the LSC-IVR and NIBA result for  $\eta/\Delta=1$ , respectively; the dot-dashed line and the triangle correspond to the LSC-IVR and NIBA result for  $\eta/\Delta=0.1$ , respectively. The other parameters used in the calculation are  $\beta\Delta=0.5$  and  $\omega_c/\Delta=10$ .

significantly below the golden-rule prediction, a typical result for the energy-diffusion regime. NIBA, on the other hand, always predicts the golden-rule rate (if the rate exists) and cannot describe such recrossing dynamics. One expects that for the spin-boson system with a more complicated spectral density, such as those that exhibit glassy behavior, NIBA would be an even worse approximation in the coherent-incoherent transition regime.

### B. The rate constant calculation

The rate constant is well-defined only if the population-spin correlation function  $P(t)$  exhibits exponential relaxation. One can fit it to an exponential form  $e^{-\alpha t}$  to obtain the rate constant  $k$  (here  $k=\alpha/2$ ), as have been done previously.<sup>20,12</sup> In practice, however, we found it more con-

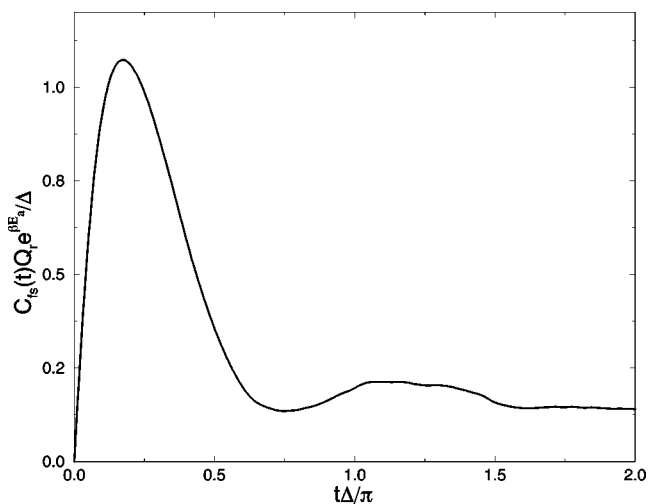


FIG. 7. Flux-side correlation function  $C_{fs}(t)$  for  $\beta\Delta=0.5$  and  $\eta/\Delta=1$ , and  $\omega_c/\Delta=10$ .

venient to use the flux correlation function formalism, Eqs. (2.17)–(2.20), to obtain the rate constant directly. The corresponding language for a well-defined rate constant is that the flux-side correlation function  $C_{fs}(t)$  can reach a stable plateau in the long time limit, and the rate is given simply as

$$k(T) = \frac{C_{fs}(t_p)}{Q_r(T)}, \quad (4.8)$$

where  $t_p$  is the plateau time and  $Q_r(T)$  is the reactant's partition function defined in Eq. (4.7). From the point of view of the flux correlation function, there are two major classes where one can identify a rate constant: the “direct” reaction and the “indirect” reaction. For the former class,  $C_{fs}(t)$  reaches its plateau in a time  $\sim\beta\hbar$  (or  $\beta\Delta$  in the units here) and stays at that plateau; whereas for the latter class,  $C_{fs}(t)$  still reaches its maximum at time  $\sim\beta\hbar$ , may or may not have a plateau, and then decreases to a smaller value. It might rise and decrease again several times, before finally reaching a stable plateau. Both of these two classes have been observed before for small gas-phase reactions,<sup>36,39–41</sup> and it is known that for the “direct” reaction case quantum transition state theory is a very good approximation for the rate constant.

For nonadiabatic transitions in the spin-boson system, the corresponding quantum transition state theory is the golden-rule:<sup>42–44</sup>

$$k_g = \beta\Delta^2 \int_{-\infty}^{\infty} dR \exp\left[-\frac{4}{\pi} \int_0^{\infty} d\omega \times \frac{J(\omega)}{\omega^2} \frac{\cosh(\beta\omega/2) - \cosh(iR\beta\omega)}{\sinh(\beta\omega/2)}\right]. \quad (4.9)$$

With the saddle point approximation for the integral over  $R$ ,<sup>43–46</sup> the expression takes the following simpler form:

$$k_g = \frac{\pi\Delta^2}{\sqrt{2 \int_0^{\infty} d\omega [J(\omega)/\sinh(\beta\omega/2)]}} \times \exp\left[-\frac{4}{\pi} \int_0^{\infty} d\omega \frac{J(\omega)}{\omega^2} \tanh(\beta\omega/4)\right]. \quad (4.10)$$

In the high temperature (small  $\beta$ ) and/or small frequency limit, the further approximations  $\tanh(\beta\omega/4) \approx \beta\omega/4$  and  $\sinh(\beta\omega/2) \approx \beta\omega/2$  can be made so that one obtains the “classical” golden-rule formula

$$k_{g,CL} = \Delta^2 \sqrt{\frac{\pi\beta}{4E_a}} e^{-\beta E_a}, \quad (4.11a)$$

where the activation energy is given by

$$E_a = \frac{1}{\pi} \int_0^{\infty} d\omega \frac{J(\omega)}{\omega}. \quad (4.11b)$$

For the Debye spectral density,  $E_a$  is equal to  $\eta/2$  as mentioned in Eq. (4.7b).

The only existing theoretical model that accounts for recrossing dynamics is Zusman's solvent dynamic model,<sup>34,23</sup>

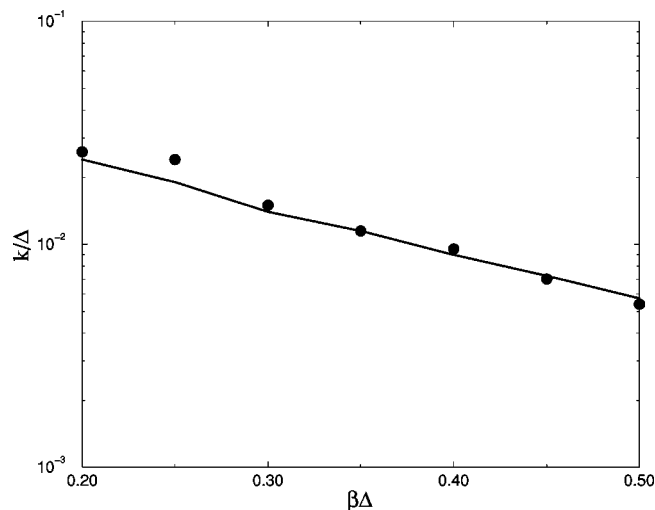


FIG. 8. Arrhenius plot of the thermal rate constant at  $\eta/\Delta=20$  and  $\omega_c/\Delta=5$ : The solid line is the golden-rule result, and the circles are results from LSC-IVR simulation.

where the diffusive motion of the bath is taken into account as a dynamical correction and the rate constant is given as

$$k_z = \frac{\Delta^2 \sqrt{\beta \pi / 4 E_a} e^{-\beta E_a}}{1 + \Delta^2 \tau_L (\pi / E_a)}, \quad (4.12)$$

and  $\tau_L = 1/\omega_c$  for the Debye spectral density. It is easy to see that in the limit of the extreme fast bath motion,  $\tau_L/\Delta \ll 1$ , the Zusman rate in Eq. (4.12) reduces to the ‘‘classical’’ golden-rule rate in Eq. (4.11a). Therefore, the limitation of Zusman’s model should be the same as the ‘‘classical’’ golden-rule, namely, high temperature and/or small characteristic frequency  $\omega_c$ . Although the small  $\omega_c$  requirement is naturally satisfied for most of the Zusman-type processes, caution must be taken in justifying the high temperature requirement.

Based on the above analysis, we summarize the LSC-IVR simulation results for the three sub-sections.

### 1. The golden-rule rate limit

This limit occurs when the coupling  $\eta$  and characteristic frequency  $\omega_c$  are sufficiently large. The temperature should not be too low, i.e., the perturbation parameter  $\beta\Delta$  should be sufficiently smaller than 1. On the other hand, to ensure the process is an activated one, the exponential parameter  $\beta E_a$  should be sufficiently large. Figure 8 is an Arrhenius plot of the calculated thermal rate constants in comparison with the golden-rule results, and they are in very good agreement. As mentioned above, this agreement is expected for this limiting case.

### 2. The Zusman rate limit

As discussed earlier, the Zusman’s model applies when the collective bath motion is slow compared with the motion of the two level system. The other requirements are similar to those in the golden-rule limit, i.e., the temperature should be high enough and the process should be an activated one. Figure 9 shows the rate constants at  $\eta/\Delta=20$  and  $\beta\Delta$

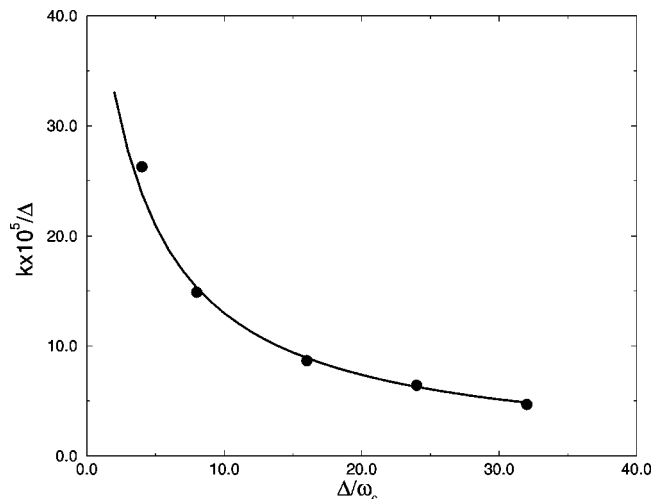


FIG. 9. Rate constant  $k/\Delta$  vs  $\Delta/\omega_c$  at  $\eta/\Delta=20$  and  $\beta\Delta=0.6$ : The solid line is the Zusman result, and the circles are results from LSC-IVR simulation.

$=0.6$ , versus the scaled relaxation time,  $\tau_L\Delta = \Delta/\omega_c$ . The solid line is from Zusman’s model, Eq. (4.12), whereas the solid circles are results from the LSC-IVR simulation. Again, they are in excellent agreement in this limiting case.

### 3. The ‘‘turnover’’ curve

This is similar to the Kramers turnover phenomenon observed for a one-dimensional double well linearly coupled to an infinite bath of harmonic oscillators. The parameter that determines the turnover is the coupling strength  $\eta$ . When  $\eta$  is extremely small, the flux correlation function displays coherent oscillations and cannot reach a plateau, and the rate constant is not defined. As  $\eta$  increases, the coupling of the bath will eventually damp the coherent motion of the two level system. Although there is still significant recrossing flux,  $C_{fs}(t)$  will reach a stable plateau in a longer time. Such a regime is called the energy-diffusion regime because energy exchange is the dominant factor. The rate constant in this regime is smaller than the transition state theory (TST) prediction. As  $\eta$  becomes even larger, the recrossing flux becomes less and the rate begins to approach the TST limit (the so-called spatial diffusion regime). However,  $\eta$  is also proportional to the activation energy so the TST rate constant tends to decrease with increase in  $\eta$ . Naturally, there is a ‘‘turnover’’ in the absolute rate constant along the  $\eta$ -axis.

Figure 10 shows the calculated rate constants versus  $\eta$  for  $\beta\Delta=0.5$  and  $\omega_c/\Delta=4$ . The turnover character is apparent. There is no analytic theory at present that explains such feature for the nonadiabatic transition process in the condensed phase. Our feeling is that this theoretical approach should be similar to the quantum turnover theory<sup>47</sup> that has been proven successful in treating the double well/infinite bath problem, and should reduce to the golden-rule formula in the spatial diffusion regime.

## V. CONCLUDING REMARKS

In this paper, a linearized approximation to the semiclassical initial value representation (LSC-IVR) has been used to

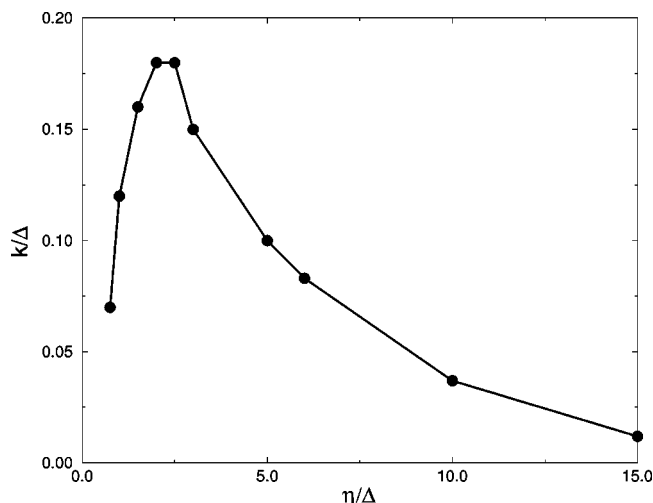


FIG. 10. Rate constants  $k/\Delta$  (solid circles) as a function of coupling parameter  $\eta/\Delta$  at  $\beta\Delta=0.5$  and  $\omega_c/\Delta=4$ . The solid line is intended simply as a guide to the eye.

study the spin-boson system with a Debye spectral density. The dynamically consistent treatment of electronic and nuclear degrees of freedom<sup>13,14</sup> is used to map the discrete spin-boson Hamiltonian into a continuous form, on which classical dynamics simulation is possible. To our knowledge, this is the first thorough numerical investigation of the spin-boson problem that covers essentially the complete parameter space, and indeed several interesting features have been observed, for the first time, from our simulation.

To summarize our results, a rough sketch of the three-dimensional phase diagram (with the three axes being the  $T$ -axis, the  $\eta$ -axis, and the  $\omega_c$ -axis) can be drawn as follows. Near the origin of the three axes, the spin-boson system exhibits coherent motion. As the phase point moves away from the origin, the overall dynamics undergoes coherent to incoherent transition. The exact cross-over position for the coherent–incoherent transition is a function of all three variables,  $T$ ,  $\eta$ , and  $\omega_c$ , since such transitions have been observed along all three axes. In the incoherent regime right after the coherent–incoherent cross-over, recrossings flux is present to some extent and thus gives a rate constant smaller than the transition state theory prediction. Until now, the only theoretical model that incorporates recrossing effects is Zusman's dynamic model,<sup>34,23</sup> which explains the dynamical behavior along the  $\omega_c$ -axis. Recrossings also exist along the other two axes and cover a broad parameter space (in fact, the parameter space that is most relevant to the chemical interest) and thus deserve more theoretical work. Only in the regime far from the origin does the incoherent relaxation give the transition state theory rate constant.

The LSC-IVR, together with the Meyer–Miller representation, offers a practical approach for simulating electronically nonadiabatic dynamics in condensed phase systems. Although the conclusions drawn in this paper are for the specific case of a Debye spectral density, we believe most of them still hold for more general spectral densities. Naturally, for a spectral density that displays complex multiple timescales, one expects an even more complicated

coherent–incoherent transition for the  $n$ -level system and a small possibility for the golden-rule formula to describe the rate accurately.

## ACKNOWLEDGMENTS

This work was supported by the Director, Office of Energy Research, Office of Basic Energy Sciences, Chemical Sciences Division of the U. S. Department of Energy under Contract No. DE-AC03-76SF00098 (HW and WHM) and No. FDDE-FG03-87ER13793 (XS and DC), by the Laboratory Directed Research and Development (LDRD) project from National Energy Research Scientific Computing (NERSC) Center, Lawrence Berkeley National Laboratory, and also by National Science Foundation Grant No. CHE 97-32758.

- <sup>1</sup>(a) W. H. Miller, in *Dynamics of Molecules and Chemical Reactions*, edited by Z. J. Zhang and R. Wyatt (Marcel Dekker, New York, 1996), p. 389; (b) W. H. Miller, *J. Phys. Chem.* **102**, 793 (1998); (c) W. H. Miller, *Faraday Discuss. Chem. Soc.* **110**, 1 (1998).
- <sup>2</sup>W. H. Miller, *J. Chem. Phys.* **53**, 3578 (1970).
- <sup>3</sup>(a) M. F. Herman and E. Kluk, *Chem. Phys.* **91**, 27 (1984); (b) E. Kluk, M. F. Herman, and H. L. Davis, *J. Chem. Phys.* **84**, 326 (1986); (c) M. F. Herman, *Chem. Phys. Lett.* **275**, 445 (1997); (d) B. E. Guerin and M. F. Herman, *ibid.* **286**, 361 (1998).
- <sup>4</sup>(a) E. J. Heller, *J. Chem. Phys.* **94**, 2723 (1991); **95**, 9431 (1991); (b) F. Grossman and E. J. Heller, *Chem. Phys. Lett.* **241**, 45 (1995).
- <sup>5</sup>K. G. Kay, *J. Chem. Phys.* **100**, 4377 (1994); **100**, 4432 (1994); **101**, 2250 (1994).
- <sup>6</sup>(a) D. Provost and P. Brumer, *Phys. Rev. Lett.* **74**, 250 (1995); (b) G. Campolieti and P. Brumer, *Phys. Rev. A* **50**, 997 (1994).
- <sup>7</sup>S. Garashchuk and D. J. Tannor, *Chem. Phys. Lett.* **262**, 477 (1996).
- <sup>8</sup>(a) A. R. Walton and D. E. Manolopoulos, *Mol. Phys.* **87**, 961 (1996); (b) A. R. Walton and D. E. Manolopoulos, *Chem. Phys. Lett.* **244**, 448 (1995); (c) M. L. Brewer, J. S. Hulme, and D. E. Manolopoulos, *J. Chem. Phys.* **106**, 4832 (1997).
- <sup>9</sup>(a) W. H. Miller, *J. Chem. Phys.* **95**, 9428 (1991); (b) B. W. Spath and W. H. Miller, *ibid.* **104**, 95 (1996); (c) X. Sun and W. H. Miller, *ibid.* **106**, 916 (1997); (d) **106**, 6346 (1997); (e) **108**, 8870 (1998).
- <sup>10</sup>D. V. Shalashilin and B. Jackson, *Chem. Phys. Lett.* **291**, 143 (1998).
- <sup>11</sup>H. Wang, X. Sun, and W. H. Miller, *J. Chem. Phys.* **108**, 9726 (1998).
- <sup>12</sup>X. Sun, H. Wang, and W. H. Miller, *J. Chem. Phys.* **109**, 7064 (1998).
- <sup>13</sup>(a) W. H. Miller and C. W. McCurdy, *J. Chem. Phys.* **69**, 5163 (1978); (b) C. W. McCurdy, H. D. Meyer, and W. H. Miller, *ibid.* **70**, 3177 (1979).
- <sup>14</sup>(a) H. D. Meyer and W. H. Miller, *J. Chem. Phys.* **70**, 3214 (1979); (b) **71**, 2156 (1979).
- <sup>15</sup>J. C. Tully, *J. Chem. Phys.* **93**, 1061 (1990).
- <sup>16</sup>A. O. Caldeira and A. J. Leggett, *Ann. Phys. (N.Y.)* **149**, 374 (1983).
- <sup>17</sup>A. J. Leggett, S. Chakravarty, A. T. Dorsey, M. P. Fisher, A. Garg, and W. Zwerger, *Rev. Mod. Phys.* **59**, 1 (1987).
- <sup>18</sup>U. Weiss, *Quantum Dissipative Systems* (World Scientific, Singapore, 1993).
- <sup>19</sup>D. E. Makarov and N. Makri, *Chem. Phys. Lett.* **221**, 482 (1994).
- <sup>20</sup>C. H. Mak and D. Chandler, *Phys. Rev. A* **44**, 2352 (1991).
- <sup>21</sup>X. Sun, H. Wang, and W. H. Miller, *J. Chem. Phys.* **109**, 4190 (1998).
- <sup>22</sup>(a) E. Pollak and J. L. Liao, *J. Chem. Phys.* **108**, 2733 (1998); (b) J. Shao, J. L. Liao, and E. Pollak, *ibid.* **108**, 9711 (1998).
- <sup>23</sup>(a) A. Garg, J. N. Onuchic, and V. Ambegaokar, *J. Chem. Phys.* **83**, 4491 (1985); (b) I. Rips and J. Jortner, *ibid.* **87**, 2090 (1987); (c) M. Spargaglione and S. Mukamel, *ibid.* **88**, 3263 (1988); (d) X. Song, Ph. D. thesis, California Institute of Technology, 1995.
- <sup>24</sup>(a) H. Weyl, *Z. Phys.* **46**, 1 (1927); (b) E. Wigner, *Phys. Rev.* **40**, 749 (1932).
- <sup>25</sup>W. H. Miller, *J. Chem. Phys.* **61**, 1823 (1974).
- <sup>26</sup>(a) E. J. Heller, *J. Chem. Phys.* **65**, 1289 (1976); (b) R. C. Brown and E. J. Heller, *ibid.* **75**, 186 (1981).
- <sup>27</sup>(a) J. S. Cao and G. A. Voth, *J. Chem. Phys.* **104**, 273 (1996); (b) R. E. Cline, Jr., and P. G. Wolynes, *ibid.* **88**, 4334 (1988); (c) V. Khidekel, V. Chernyak, and S. Mukamel, in *Femtochemistry: Ultrafast Chemical and Physical Processes in Molecular Systems*, edited by M. Chergui

- (World Scientific, Singapore, 1996), p. 507; (d) H. W. Lee and M. O. Scully, *J. Chem. Phys.* **73**, 2238 (1980).
- <sup>28</sup>(a) V. S. Filinov, V. V. Medvedev, and V. L. Kamskyi, *Mol. Phys.* **85**, 711 (1995); (b) V. S. Filinov, *ibid.* **88**, 71517 (1996); (c) **88**, 1529 (1996).
- <sup>29</sup>(a) R. B. Gerber, V. Buch, and M. A. Ratner, *J. Chem. Phys.* **77**, 3022 (1982); (b) V. Buch, R. B. Gerber, and M. A. Ratner, *Chem. Phys. Lett.* **101**, 44 (1983).
- <sup>30</sup>(a) R. K. Preston and J. C. Tully, *J. Chem. Phys.* **54**, 4297 (1971); (b) **55**, 562 (1971); (c) M. F. Herman, *ibid.* **76**, 2949 (1982).
- <sup>31</sup>G. Stock and M. Thoss, *Phys. Rev. Lett.* **78**, 578 (1997).
- <sup>32</sup>(a) W. H. Miller, *J. Chem. Phys.* **61**, 1823 (1974); (b) W. H. Miller, S. D. Schwartz, and J. W. Tromp, *ibid.* **79**, 4889 (1983).
- <sup>33</sup>See also, T. Yamamoto, *J. Chem. Phys.* **33**, 281 (1960).
- <sup>34</sup>L. D. Zusman, *Chem. Phys.* **49**, 295 (1980).
- <sup>35</sup>(a) B. Carmeli and D. Chandler, *J. Chem. Phys.* **82**, 3400 (1985); (b) J. N. Gehlen and D. Chandler, *ibid.* **97**, 4958 (1992).
- <sup>36</sup>H. Wang, W. H. Thompson, and W. H. Miller, *J. Chem. Phys.* **107**, 7194 (1997).
- <sup>37</sup>(a) E. M. Kosower and D. Huppert, *Annu. Rev. Phys. Chem.* **37**, 127 (1986); (b) M. Weaver and T. Gennet, *Chem. Phys. Lett.* **113**, 213 (1985); (c) S. G. Su and J. D. Simon, *J. Phys. Chem.* **90**, 6457 (1986); (d) M. McGuire and G. McLendon, *ibid.* **90**, 2549 (1986).
- <sup>38</sup>C. Aslangul, N. Pottier, and D. Saint-James, *J. Phys. (Paris), Colloq.* **47**, 1657 (1986).
- <sup>39</sup>W. H. Thompson and W. H. Miller, *J. Chem. Phys.* **106**, 142 (1997); **107**, 2164(E) (1997).
- <sup>40</sup>T. C. Germann and W. H. Miller, *J. Phys. Chem.* **101**, 6358 (1997).
- <sup>41</sup>H. Wang, W. H. Thompson, and W. H. Miller, *J. Phys. Chem. A* **102**, 9372 (1998).
- <sup>42</sup>(a) V. G. Levich and R. R. Dogonadze, *Dokl. Akad. Nauk SSSR* **124**, 123 (1959); (b) A. A. Ovchinnikov and M. Ya. Ovchinnikova, *Sov. Phys. JETP* **29**, 688 (1969); (c) R. R. Dogonadze, A. M. Kuznetsov, and T. A. M. Marsagishvili, *Electrochim. Acta* **25**, 1 (1980).
- <sup>43</sup>J. Ulstrup, *Charge Transfer in Condensed Media* (Springer, Berlin, 1979).
- <sup>44</sup>R. A. Kuharski, J. S. Bader, D. Chandler, M. Spirk, M. L. Klein, and R. W. Impey, *J. Chem. Phys.* **89**, 3248 (1988); J. S. Bader, R. A. Kuharski, and D. Chandler, *ibid.* **93**, 230 (1990).
- <sup>45</sup>X. Song and A. A. Stuchebrukhov, *J. Chem. Phys.* **99**, 969 (1993).
- <sup>46</sup>X. Song and R. A. Marcus, *J. Chem. Phys.* **99**, 7768 (1993).
- <sup>47</sup>E. Pollak, H. Grabert, and P. Hänggi, *J. Chem. Phys.* **91**, 4073 (1989).